Geochemistry, Geophysics, Geosystems

RESEARCH ARTICLE
10.1029/2019GC008193

Ce/Mo and Molybdenum Isotope Systematics in Subduction-Related Orogenic Potassic Magmas of Central-Southern Italy

M. Casalini[1,2], R. Avanzinelli[1,3], S. Tommasini[1], T. Elliott[2], and S. Conticelli[1,3,4]

[1]Dipartimento di Scienze della Terra, Università degli Studi di Firenze, Florence, Italy, [2]School of Earth Sciences, University of Bristol, Bristol, UK, [3]Istituto di Geoscienze e Georisorse, Consiglio Nazionale delle Ricerche, Florence, Italy, [4]Istituto di Geologia Ambientale e Geoingegneria, Monterotondo, Italy

Key Points:
- Mo isotopic compositions of Italian potassic and ultrapotassic magmas are among the heaviest recorded so far in subduction-related lavas
- Isotopically heavy Mo isotopic sedimentary components are required for mantle source metasomatism with negligible, if any, Mo isotope fractionation
- Residual sulfides±rutile versus epidote and Ca-poor versus Ca-rich subducted sediments are key in controlling Ce/Mo fractionation during melting

Supporting Information:
- Supporting Information S1
- Table S1
- Table S2
- Table S3

Correspondence to:
R. Avanzinelli and S. Conticelli,
riccardo.avanzinelli@unifi.it;
sandro.conticelli@unifi.it

Citation:
Casalini, M., Avanzinelli, R., Tommasini, S., Elliott, T., & Conticelli, S. (2019). Ce/Mo and molybdenum isotope systematics in subduction-related orogenic potassic magmas of Central-Southern Italy. *Geochemistry, Geophysics, Geosystems*, *20*. https://doi.org/10.1029/2019GC008193

Received 9 JAN 2019
Accepted 27 APR 2019
Accepted article online 13 MAY 2019

Abstract Several recent studies have employed variations in the concentration and isotopic composition of molybdenum as tracers of igneous processes. In this study we present new Mo concentration and $\delta^{98/95}$Mo data on the peculiar subduction-related potassic magmas of the Central-Southern Italian peninsula; the leucite-free (lamproite-like) rocks of the Tuscan Magmatic Province and the leucite-bearing rocks of Mt. Vesuvius. These rocks display exotic and distinctive geochemical and isotopic features due to differences in the lithology of the subducted material in their respective mantle sources. We examine the elemental and isotopic systematics of Mo in the context of these geochemical variations. The two different associations of magmas display significantly different Ce/Mo values but surprisingly similar $\delta^{98/95}$Mo values (0.10–0.26‰ for Vesuvius and 0.07–0.24‰ for Tuscan Magmatic Province), which are significantly heavier than typical mid-ocean ridge basalts. While the $\delta^{98/95}$Mo implicate an isotopically heavy sedimentary component recycled into their respective mantle sources, the different Ce/Mo ratios reflect contrasting elemental fractionation during sediment melting related to the lithology and consequent residual mineralogy (sulfides vs. epidote) of the subducted sedimentary material undergoing melting (Ca poor vs. Ca rich). This indicates that the heavy Mo isotopic signature of these magmas is independent of the lithology of the recycled material, which instead controls the elemental fractionation of Mo.

Plain Language Summary Subduction is one of the most important processes of plate tectonics and controls the global cycle of elements from surface to Earth's interior. Recycling via subduction is an efficient mechanism for returning light and incompatible trace elements to the mantle. Trace elements and isotopic compositions represent a unique tool for investigating the different components in defining the geochemical signature of orogenic magmas. We apply the study of Mo elemental and isotopic systematics to some Italian potassic volcanic rocks (i.e., leucite-free rocks from Tuscany and leucite-bearing rocks from Vesuvius), which are from mantle sources clearly dominated by different recycled sediments (carbonate poor vs. carbonate rich). Mo isotope compositions of these two groups are similar, at odds with the significantly different trace element and radiogenic isotope signature, and are also among the heaviest recorded in subduction-related magmas arguing for originally heavy recycled sediment components. The distribution of Mo, Ce, and Nb between the two groups requires specific fractionation that can be explained by the role of different accessory phases (sulfides vs. epidote) occurring as residual phases after sediment melting. We present a model to constrain the process liable to reproduce the melt components responsible for mantle metasomatism of the studied rocks.

1. Introduction

Subduction zones represent the primary geological setting where the oceanic crust (basalts and sediments) and possibly the continental crust are recycled into our planet's interior. Subduction-related volcanic rocks bear specific geochemical signatures recording the type of materials recycled and the nature of their transport into the mantle; slab-derived fluids with radiogenic isotope compositions similar to that of mafic oceanic crust and slab-derived melts inferred to be derived from recycling of subducted sediments (e.g., Elliott, 2003; Hawkesworth et al., 1993, 1997; Plank, 2005; Plank & Langmuir, 1993).

In the last decade, "non-traditional" Mo stable isotopic systematics were explored to obtain new insights into the generation of these slab components at subduction zones (Freymuth et al., 2015, 2016; Gaschnig et al.,

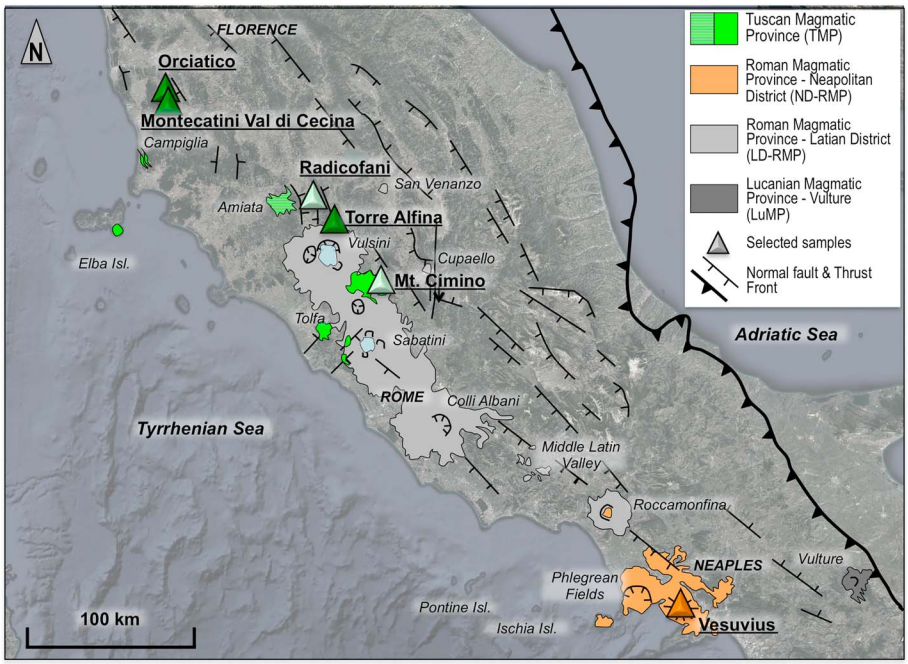

Figure 1. Schematic map of the potassic and ultrapotassic associations of magmas outcropping on the Tyrrhenian border of the Italian peninsula. The Tuscan Magmatic Province (TMP) samples are dark green (lamproite) and light green (shoshonite/calc-alkaline) triangles, while Mt. Vesuvius samples are represented by an orange triangle. Outlines of other volcanic outcrops from the Latium District of the Roman Magmatic Province and the Lucanian Magmatic Province are reported in gray (see Conticelli et al., 2015, for a review).

2017; König et al., 2016; Voegelin et al., 2014; Wille et al., 2018). Fluid-dominated arcs are generally characterized by high $\delta^{98/95}$Mo (Freymuth et al., 2015; König et al., 2016), while sediment-dominated subduction-related magmas have variable Mo isotopic signatures from light (e.g., Cyprus and Papua New Guinea; König et al., 2016) to heavy (Aegean, Voegelin et al., 2014, Lesser Antilles, Freymuth et al., 2016, Banda, Wille et al., 2018).

The reasons for the variability of Mo isotopic compositions in subduction zone lavas remain a matter of debate. In this study, we report new Mo isotope data on potassic and ultrapotassic mafic rocks produced at destructive plate margins by partial melting of mantle sources strongly modified by large amounts of recycled sediments (e.g., Casalini et al., 2017, 2018; Conticelli & Peccerillo, 1992; Conticelli et al., 2013, 2015; Prelević & Foley, 2007; Prelević et al., 2006). The aim is to add a new piece to the Mo isotope puzzle, investigating two contrasting cases of subduction-related orogenic potassic magmas from Central-Southern Italian peninsula: the leucite-free lamproite-like rocks of the Tuscan Magmatic Province (hereafter TMP), in Central Italy, and the leucite-bearing rocks of Mt. Vesuvius, in Southern Italy (Figure 1).

Both occurrences have long been studied due to their exotic compositions, which display both mantle- and crust-like geochemical characteristics. Many previous studies have extensively debated when and where the marked crustal signatures of these rocks were acquired. It is now widely accepted that the genesis of these potassic magmas is due to the dominant role of recycled sediment melt addition to their sources within the mantle wedge (e.g., Avanzinelli et al., 2008, 2009, 2018; Ayuso et al., 1998; Conticelli & Peccerillo, 1992; Conticelli et al., 2013, 2015; D'Antonio et al., 1999; Foley, 1992; Iovine et al., 2018; Peccerillo, 1998, 2001, 2017).

The compositions of the magmas, however, reveal a significant difference in the lithologies of the subducted materials contributing to the sources of the two suites, with carbonate-rich sediments recycled beneath Mt. Vesuvius compared to siliciclastic, carbonate-poor, sediments recycled into the mantle beneath the TMP (e.g., Avanzinelli et al., 2009, 2018; Conticelli et al., 2011, 2015; Peccerillo, 2017). Such a difference is liable to control the residual phase mineralogy during sediment melting (Avanzinelli et al., 2009, 2018) and can potentially add new constraints to the fate of Mo and its isotopes during subduction and recycling of

sediments at convergent margins. In order to better constrain the mantle enrichment process via sediment melting, we also present data on selected sedimentary material representative of that subducted underneath the two regions.

2. Molybdenum Isotope Systematics at Subduction Zone

Molybdenum is a transition metal occurring in nature with several valence states, including Mo^{4+} and Mo^{6+}. Mo^{6+} is the dominant species in partial melts (O'Neill & Eggins, 2002) and in oxic aqueous environments. During chemical weathering of continental crust, the soluble molybdate species (MoO_4^{-2}) can be easily transported to the ocean. Similarly, it was proposed that Mo could be mobilized from the subducting slab during its dehydration (Freymuth et al., 2015; König et al., 2010), although Noll et al. (1996) argued that Mo could be largely immobile in fluids from the subducting slab. Mo forms a number of particle reactive sulfide compounds, which leads to strong Mo enrichment in sediments deposited in sulfidic conditions such as black shales (e.g., Bertine & Turekian, 1973) although the exact processes for Mo scavenging are still not clear (see Kendall et al., 2017 for review).

Molybdenum has seven stable isotopes, two of which are used in the conventional δ notation ($\delta^{98/95}Mo = [(^{98}Mo/^{95}Mo_{sample}/^{98}Mo/^{95}Mo_{NIST3134}) - 1]$). Mo isotopes experience notable mass-dependent isotopic fractionation in natural systems, allowing their use as paleoproxy for oceanic redox conditions (e.g., Barling et al., 2001; Siebert et al., 2003). In oxic conditions Mo is dissolved in seawater and it is partially absorbed onto Fe-Mn oxides, which preferentially incorporate light Mo isotopes. Relatively low $\delta^{98/95}Mo$ are also reported for suboxic or mildly anoxic sedimentary environments, due to nonquantitative absorption processes. On the other hand, in strongly reducing conditions, Mo is quantitatively scavenged from seawater into anoxic sediments, without any significant isotopic fractionation, as shown by the isotopically heavy Mo recorded in black shales (e.g., Arnold et al., 2004; Barling et al., 2001; Neubert et al., 2008). The occurrence of isotopically distinct reservoirs of superficial Mo in sediments that are then recycled into the mantle raised the interest in the use of Mo isotopes as tracers in subduction zones (e.g., Freymuth et al., 2016).

Some studies (e.g., Voegelin et al., 2014; Wille et al., 2018) suggested that differentiation of high-temperature hydrous magmas results in measurable isotopic fractionations, although at much smaller magnitude than the fractionations observed in low-temperature environments. On the other hand, work on Iceland (Yang et al., 2015) and other studies on subduction-related settings (e.g., Casalini, 2018; Freymuth et al., 2015; Gaschnig et al., 2017) found no evidence indicating $\delta^{98/95}Mo$ fractionation during magma differentiation, but the latter did identify Mo isotopic fractionation during the processes of their genesis. Freymuth et al. (2015) accounted for the generally high $\delta^{98/95}Mo$ measured in the Mariana arc lavas as due to the addition of fluids expelled from the subducting basaltic crust. They tentatively suggested that high $\delta^{98/95}Mo$ was produced by fractionation of Mo between fluid and residual rutile during slab dehydration, with rutile retaining the lighter Mo isotopes. Similar inferences were made by König et al. (2016) on rocks from different volcanic arcs (Solomon arc and Bismark arc) and subduction-related settings (e.g., Cyprus). The low $\delta^{98/95}Mo$ of the lavas from Cyprus was explained by the breakdown of residual rutile and release of isotopically light Mo (König et al., 2016).

Alternatively, the isotopic composition of erupted magmas may reflect the original $\delta^{98/95}Mo$ of the subducted sediment, with little or no fractionation during subduction (Freymuth et al., 2016; Gaschnig et al., 2017). These two independent studies on sediment-dominated lavas from the Lesser Antilles highlighted that high $\delta^{98/95}Mo$ is inherited directly from either the subducted anoxic black shales or recycling of their melts into the mantle wedge, whereas the low $\delta^{98/95}Mo$ values are derived from the involvement oxic-suboxic isotopically light sediments (Freymuth et al., 2016; Gaschnig et al., 2017). Further information on this scenario is provided by a recent experimental study of Skora et al. (2017) carried out on sediments similar to those invoked to metasomatize the mantle wedge of the Lesser Antilles.

3. Materials and Methods

3.1. Volcanic Rocks

The studied samples belong to two Italian potassic-ultrapotassic associations, namely, the TMP, which consists of leucite-free potassic to ultrapotassic igneous rocks emplaced from Miocene to Lower Pleistocene in

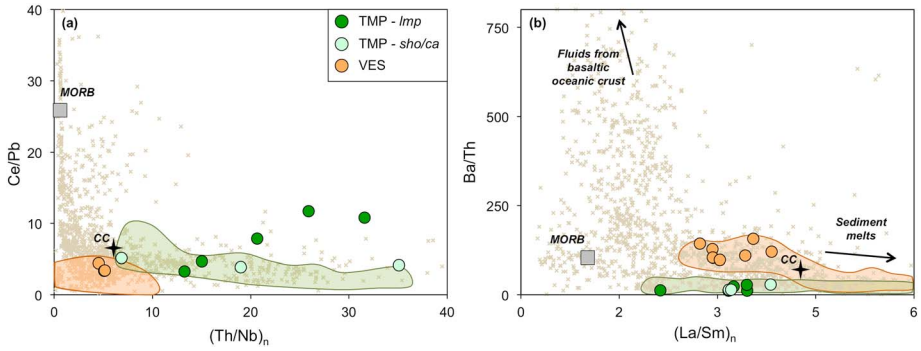

Figure 2. $(Th/Nb)_n$ versus Ce/Pb (a) and $(La/Sm)_n$ versus Ba/Th (b) of the studied magmas. Ce and Th contents dominate the Ce/Pb and Th/Nb of Vesuvius and Tuscan magmas, respectively (see also Figure 7 and Table S1). Colored fields refer to Tuscan and Vesuvius magmas from literature (see Conticelli et al., 2015, for a review). Other arcs, reported for comparison, are from GeoRoc database (georoc.mpch-mainz.gwdg.de/georoc/). The MORB value represents the average of compilation of global MORB data from Gale et al. (2013). The CC (continental crust) composition is from Rudnick and Gao (2014).

Southern Tuscany and Northern Latium (e.g., Conticelli et al., 2009, 2011, 2013) and Mt. Vesuvius in the Neapolitan District of the Roman Province, which consists of leucite-bearing volcanic rocks erupted from Middle Pleistocene to Holocene (Avanzinelli et al., 2018; Ayuso et al., 1998; Cioni et al., 2008; Santacroce et al., 1993; Figure 1). Both associations are enriched in incompatible trace elements, with a marked subduction-related signature (i.e., low Ce/Pb and high $(Th/Nb)_n$, Figure 2a), and plot within the sediment-dominated sector of the a Ba/Th versus $(La/Sm)_n$ diagram (Figure 2b) used to discriminate mantle wedge metasomatism by subducting slab fluids versus melts (Elliott, 2003).

Despite these generally similar characteristics, the two magmatic provinces differ in terms of degree of silica saturation, trace element ratios, and radiogenic isotope (Sr, Nd, and Pb) signatures. These differences have long been discussed and investigated starting from the early twentieth century, on the basis of geochemical and mineralogical compositions (e.g., Washington, 1906), and then later with the addition of isotope composition (e.g., Savelli, 1967; Vollmer, 1976); we refer to the comprehensive recent reviews of Conticelli et al. (2010, 2015) and Peccerillo (2017) for details on their elemental and traditional isotopic characteristics and geodynamic implications. The key difference between the two associations of magmas is the change in nature and composition of the subducted crustal material contributing to their mantle sources (Figure 3). Terrigenous siliciclastic sediments are the dominant subducted material added to the lithospheric mantle source of the leucite-free ultrapotassic rocks of the TMP (e.g., Avanzinelli et al., 2009; Conticelli & Peccerillo, 1992; Conticelli et al., 2004, 2009, 2013, 2015), while a two-step metasomatic process was recently invoked to account for the mantle wedge composition beneath Mt. Vesuvius (Avanzinelli et al., 2018). The first step consists of melts from a slab-derived component (basalt + siliciclastic) similar to that metasomatizing the mantle wedge of the neighboring Stromboli volcano; the second step consists of melts from a slab-derived marly component, responsible for values of $(^{238}U/^{230}Th)>1$ recorded in Mt. Vesuvius magmas (Avanzinelli et al., 2008, 2018).

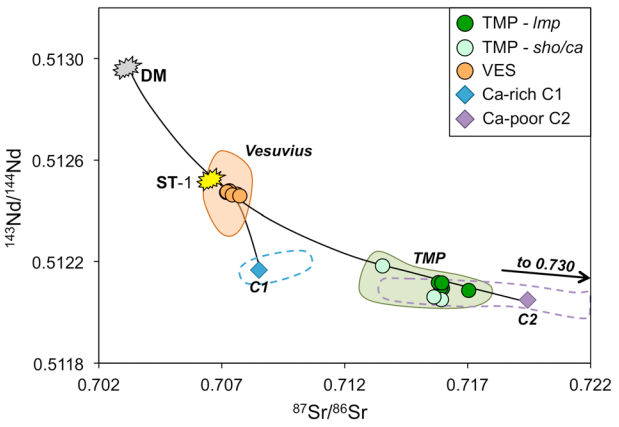

Figure 3. $^{87}Sr/^{86}Sr$ versus $^{144}Nd/^{143}Nd$ of Tuscan Magmatic Province (TMP) and Mt. Vesuvius magmas. Colored fields refer to Tuscan and Vesuvius magmas from literature (see Conticelli et al., 2015). Tuscan Magmatic Province (TMP) magmas are modeled by a mixing curve between a depleted mantle source (DM) and the Ca-poor siliciclastic sediment composite C2 (see text for details). Vesuvius magmas are modeled according to the two-step metasomatic process reported in Avanzinelli et al. (2018). The composition of the mantle source after the first step I (ST-1: yellow symbol) taken from Avanzinelli et al. (2018) falls along the mixing curve between DM and C2. The second step is modeled as a mixing between ST-1 and the Ca-rich sediment C1 (see text for details). The compositions of other sediment components used in the literature are reported, for comparison, as dashed fields (Avanzinelli et al., 2018; Conticelli et al., 2015).

All samples were selected from a group of well-characterized rocks. Lucite-free ultrapotassic rocks of the TMP rocks show petrographic and geochemical characteristics indicating no crustal contamination occurred in the most mafic samples (e.g., Ammannati et al., 2016; Conticelli, 1998; Conticelli et al., 2015). At Vesuvius, on the other hand, a significant role for crustal contamination was suggested (e.g., Iacono-Marziano et al.,

2009; Pichavant et al., 2014) although Avanzinelli et al. (2018) showed, on the basis of U-series disequilibria and $\delta^{238/235}U$, that such a process has little effect, if any, on the overall trace element abundances and radiogenic isotope signatures of leucite-bearing Vesuvius lavas.

Eight representative samples of the most mafic volcanic rocks of the TMP were selected from either subvolcanic bodies or small lava flows (Figure 1). In order to include in the data set all the different series occurring in the area, we selected, on the basis of their K_2O content, five lamproites, two shoshonites, and one high-K calc-alkaline basalt (Tables S1 and S2 in the supporting information). Lamproite samples are from Orciatico (4.1 Ma), Montecatini val di Cecina (4.1 Ma), and Torre Alfina (0.88 Ma) centers (dark green symbols in all diagrams); shoshonites and the high-K calc-alkaline basalt are from Monte Cimino (0.98 Ma) and Radicofani (1.2 Ma) volcanoes (light green symbols in all diagrams). All samples (see Table S1) are silica saturated, have high Mg# [mol MgO/(MgO+FeO_{tot})], and preserve a "primitive" character as testified by mineralogical and petrologic characteristics (e.g., Ammannati et al., 2016; Conticelli et al., 2011, 2013, 2015; Foley, 1992; Peccerillo, 2017). Their trace element contents display a typical subduction-related pattern characterized by high Large-Ion Lithophile Elements/High Field Strength Elements ratios (e.g., Figure 2a), while their Sr, Nd, and Pb isotope compositions (e.g., Figure 3) indicate recycling of a siliciclastic crustal component to their mantle source (e.g., Conticelli & Peccerillo, 1992; Conticelli et al., 2009, 2011, 2013, 2015; Gasperini et al., 2002, and references therein). The seven samples from Vesuvius were selected from a suite of mafic lava flows of the 1631–1944 Common Era period of activity and are silica-undersaturated leucite-bearing rocks, recently reported and discussed in Avanzinelli et al. (2018). The Mt. Vesuvius volcanic edifice belongs to Neapolitan District, the southernmost and youngest volcanic products of the Roman Magmatic Province (Conticelli et al., 2015; Figure 1). The samples have less extreme compositional characteristics, with more moderate trace element enrichment, lower Large-Ion Lithophile Elements/High Field Strength Elements ratios (Figure 2a), lower Sr and Pb, and higher Nd isotope compositions than TMP rocks (Figure 3), along with ($^{238}U/^{230}Th$)>1.

3.2. Sedimentary Rocks

The Tethyan oceanic plate has been totally consumed beneath the European plate, and the only remnants are represented by nappes (i.e., Ligurides; Vai & Martini, 2013) outcropping along the Apennine belt, which were obducted onto the Adria plate during the Miocene anticlockwise rotation of the European plate (e.g., Faccenna et al., 2001; Vai & Martini, 2013).

Hence, to investigate the influence of recycled sedimentary material on the Mo isotopic composition of the studied magmas, we have selected and analyzed several samples outcropping on the nearby transect of the Apennine chain and representing a complete section of the obducted Tethyan oceanic crust from mafic peridotite at the bottom to thick layers of Ca-rich sedimentary rocks (e.g., *Calpionella* Limestone, Vai & Martini, 2001) and pelagic Ca-poor shales and turbidites (e.g., *Palombini* Shales, *Val di Vara* Supergroup, Vai & Martini, 2013), at the top of the log. The samples collected (Tables S1 and S2) are likely analogues of the subducted sedimentary lithologies that are responsible for mantle source enrichment of the TMP and Vesuvius magmas.

3.3. Analytical Methods

Sample preparation and measurements were performed at the University of Bristol using a ThermoFinnigan Neptune™ multicollector inductively coupled plasma mass spectrometer. The instrument is equipped with nine Faraday cups connected to feedback amplifiers with 10^{11} Ω resistors. Operational settings, Mo isotopic composition, and Mo concentration with the double spike technique are from Willbold et al. (2016). A ^{97}Mo-^{100}Mo double spike was employed in this study and was added to all samples before the dissolution. The chemical procedure used to purify Mo from the matrix element consisted of a single anionic exchange column step in low aspect ratio Bio-Rad "Poly-prep" columns filled with AG1x8 (100–200 mesh) resin (Willbold et al., 2016). This procedure allows an efficient removal of most of the matrix and those elements causing isobaric interferences (such as Ru). Sediments or large samples were loaded onto 2 ml anion exchange resin, whereas lava samples were loaded onto 1 ml resin adjusting eluting acid volumes accordingly. All the sedimentary rocks were treated before acid digestion with concentrated HNO_3 and H_2O_2 to remove organics.

$^{98}Mo/^{95}Mo$ isotopic composition of samples reported in this paper is parts per thousand deviation relative to the international reference solution NIST 3134 released by the National Institute of Standards and

Technology (NIST) (Goldberg et al., 2013; Greber et al., 2012). Our sample and reference sample solutions had the same concentration during measurements (300–400 ppb), yielding some 7×10^{-11} A ion currents for ^{98}Mo. The typical inlet instrument setting used, includes a combination of Aridus desolvating system, PFA nebulizer (nominal 50 μl/min) and Ni "h-type" skimmer cones.

All the sessions were preceded by measurements of three aliquots of NIST reference material mixed with the ^{97}Mo-^{100}Mo double spike in solution/spike ratios ranging from 2:1 to 1:2 to assess the effect of variable sample/spike ratio on the accuracy of the determined Mo isotope ratios.

The external reproducibility on replicate analyses of the arc basalt JB-2 international reference sample (one aliquot in each batch of samples) yielded $\delta^{98/95}$Mo = 0.052 ± 0.031‰ and Mo = 0.897 ± 0.026 ppm (n = 19, Table 1), in agreement with literature data (Freymuth et al., 2015; Willbold et al., 2016). The uncertainties reported for JB-2 reference sample represent 2σ standard deviations of repeated measurements and so are indicative of the reproducibility of the unknown samples.

Total procedural blanks over the period of measurements were <100 pg for small size samples (<100 mg powder, separated on 1 ml column volume, n = 7) and <200 pg for large samples (up to 1.5 g, separated on 2 ml column volume, n = 3), well within the acceptable range suggested by Willbold et al. (2016). Each duplicate analysis reported in Table 1 (as *rep*) consists of a repeat of the entire procedure from the same powered rock sample.

4. Results

4.1. Volcanic Rocks

The results of Mo isotopic composition and Mo concentration on the studied samples are reported in Table 1; the full data set for each sample is provided as supporting information (Tables S1 and S2).

In general, Ce/Mo of arc magmas has been suggested to be either near constant (Noll et al., 1996) and similar to Middle Ocean Ridge Basalt (MORB) values (~30: Gale et al., 2013) or to be lowered by the relatively high mobility of Mo than Ce in slab-derived fluids (Bali et al., 2012; Freymuth et al., 2015; König et al., 2010, 2016). In fact, our data show an opposite behavior of Mo and Ce between TMP and Mt. Vesuvius rocks (Figure 4). The magmatic products from the former show variable and consistently high Ce/Mo at low Mo contents (Figure 4a) and are significantly different from all other subduction-related magmas reported so far. The lamproites (ultrapotassic leucite-free rocks) have slightly higher Mo than shoshonites (potassic leucite free), and more than twofold Ce/Mo variation within the TMP samples (Ce/Mo = 170–350) is dominated by Ce abundance variability (Figure 4a). The variable Ce/Mo of these rocks (Figure 4a) is at odds with the similar degree of incompatibility of Mo and Ce during mantle melting (Newsom et al., 1986; Noll et al., 1996; Sims et al., 1990) and demands that unique metasomatic processes affect their mantle sources.

On the other hand, the Vesuvius samples show significantly lower and less variable Ce/Mo values (25 on average) than Tuscan magmas, similar to some other subduction-related magmas yet with higher Ce and Mo absolute contents. In this case, Ce/Mo is controlled by Mo content, which is higher than in the TMP rocks (3.02–4.91 ppm), while Ce remains almost constant (~100 ppm; Figure 4a). There is no correlation between Ce/Mo and MgO content (Figure 4b), suggesting that this elemental ratio is not influenced by magmatic differentiation and reflects the original heterogeneity of the magma source linked to the nature of the material involved during subduction and to the processes responsible for its recycling.

Despite their significant differences in trace elements (e.g., Ce, Mo, and Ce/Mo) and radiogenic isotope compositions (Figure 3 and Tables S1 and S2; see also Conticelli et al., 2015 for a review), the two Italian magmatic associations show strikingly similar $\delta^{98/95}$Mo compositions (Figure 4c). Indeed, all the analyzed magmas outline a relatively narrow $\delta^{98/95}$Mo range, with values between 0.10‰ and 0.26‰ for Vesuvius and 0.07‰ and 0.24‰ for Tuscan magmas, covering a total range of $\Delta^{98/95}$Mo of 0.18‰ (Table 1). The studied magmas have considerably higher $\delta^{98/95}$Mo than MORBs (Bezard et al., 2016; Freymuth et al., 2015; Liang et al., 2017) and are among the heaviest Mo isotope compositions recorded so far in subduction-related magmas (e.g., Aegean arc, Cyprus, Marianas, Solomon Islands, and Papua New Guinea; Freymuth et al., 2015; König et al., 2016; Voegelin et al., 2014; Figure 4c). The $\delta^{98/95}$Mo of TMP and Vesuvius magmas are comparable to the isotopically heaviest samples from the Lesser Antilles arc, Kos Plateau Tuff, and Banda arc. Intriguingly, in the first

Table 1
Mo Isotope Compositions and Mo Content of Tuscan Magmatic Province and Mt. Vesuvius Magmas

Sample name	Outcrop	Instrument-laboratory	$\delta^{98/95}$Mo (‰)	2 s.e.	Mo (ppm)	Ce/Mo	MgO (wt. %)
Tuscan province							
MVC100	Plug	MC-ICPMS-BIG	0.223	±0.029	1.19	173	7.15
rep			*0.266*	*±0.027*			
avg			*0.245*				
ORC 01	Laccolith	MC-ICPMS-BIG	0.130	±0.030	1.14	308	8.23
ORC 04	Laccolith	MC-ICPMS-BIG	0.138	±0.019	1.15	247	8.27
rep			*0.096*	*±0.037*			
avg			*0.117*				
VS 123	Lava flow	MC-ICPMS-BIG	0.138	±0.021	0.57	181	7.82
rep			*0.110*	*±0.044*			
avg			*0.124*				
VS 114	Lava flow	MC-ICPMS-BIG	0.169	±0.028	0.64	236	9.09
rep			*0.163*	*±0.042*			
avg			*0.166*				
VS 184	Lava flow	MC-ICPMS-BIG	0.146	±0.018	0.53	340	9.48
rep			*0.166*	*±0.030*			
avg			*0.156*				
VS 29	Lava flow	MC-ICPMS-BIG	0.081	±0.024	1.30	191	9.36
rep			*0.081*	*±0.024*			
avg			*0.081*				
VS 28	Lava flow	MC-ICPMS-BIG	0.073	± 0.026	1.30	175	8.72
Vesuvius							
VES 01	Lava Flow	MC-ICPMS-BIG	0.133	± 0.028	3.28	29	4.49
VES 07	Lava Flow	MC-ICPMS-BIG	0.172	± 0.028	4.34	23	3.96
VES 18	Lava Flow	MC-ICPMS-BIG	0.175	± 0.021	3.76	26	3.02
VES 16	Lava Flow	MC-ICPMS-BIG	0.098	±0.023	3.02	31	4.80
VES 17	Lava Flow	MC-ICPMS-BIG	0.134	±0.029	3.91	26	3.71
97VS718b	Scoria	MC-ICPMS-BIG	0.239	±0.023	3.55	27	7.45
95VS135	Scoria	MC-ICPMS-BIG	0.257	±0.025	4.91	21	4.36
Sediments	Lithology						
SD 47	Carbonate-rich marlstone	MC-ICPMS-BIG	0.728	±0.028	0.47	28	
SD 44	Carbonate-rich marlstone	MC-ICPMS-BIG	−0.444	±0.048	0.43	53	
SD 48	Carbonate-rich marlstone	MC-ICPMS-BIG	−2.016	±0.039	0.58	41	
SD 34	Carbonate-rich marlstone	MC-ICPMS-BIG	−1.013	±0.031	0.22	220	
a			*−1.031*	*±0.058*			
b			*−1.013*	*±0.026*			
SD 53	Carbonate-rich marlstone	MC-ICPMS-BIG	−0.469	±0.021	0.22	221	
a			*−0.723*	*±0.099*			
b			*−0.469*	*±0.031*			
SD 11	Carbonate-rich marlstone	MC-ICPMS-BIG	0.586	±0.033	0.42	103	
SD 41	Carbonate-poor marlstone	MC-ICPMS-BIG	−0.463	±0.033	0.11	580	
SD 55	Carbonate-poor marlstone	MC-ICPMS-BIG	−0.260	±0.034	0.19	339	
b			*−0.260*	*±0.021*			
SD 42	Carbonate-poor marlstone	MC-ICPMS-BIG	−0.299	±0.036	1.04	38	
SD 75	Carbonate-poor marlstone	MC-ICPMS-BIG	0.491	±0.026	0.54	129	
			0.461	*±0.062*			
b			*0.491*	*±0.036*			

Table 1 *(continued)*

Sample name		Outcrop	Instrument-laboratory	$\delta^{98/95}$Mo (‰)	2 s.e.	Mo (ppm)	Ce/Mo	MgO (wt. %)
SD 62 [b]		Carbonate-poor marlstone	MC-ICPMS-BIG	1.066 *1.066*	±0.032 *±0.034*	1.10	82	
Composites		$^{87}Sr/^{86}Sr$	$^{143}Nd/^{144}Nd$					
C1a	Ca- rich	0.70851	0.51217	0.38		0.40	84	
C1b	Ca- rich	0.70851	0.51217	−0.05		0.40	85	
C2	Ca- poor	0.71944	0.51205	0.30		0.37	176	
Reproducibility of international standards				$\delta^{98/95}$Mo	2σ (#)	Mo		
JB-2			MC-ICPMSBIG	0.052	±0.031 (19)	0.89		

Note. $\delta^{98/95}$Mo were measured by isotope dilution using well-established techniques (Willbold et al., 2016) at BIG via MC-ICP-MS using a ^{97}Mo-^{100}Mo double spike solution and a Matlab deconvolution for mass bias correction. All the measurements are normalized compared to the NIST 3134 as a reference standard solution. Internal errors on sample data (±2 s.e.) are fully propagated for the reference sample correction. Reproducibility of international Reference Standard Material JB-2 is expressed as 2σ; (#) = number of analyses. The fully propagated internal error (2 s.e.) on the $n = 19$ measured replicates of the JB-2 standard was on average 0.027. Replicates (in italic) are made on completely separate sample dissolutions; averages of the two replicates are also reported. MC-ICP-MS = multicollector inductively coupled plasma mass spectrometer.
[a]HPA digestion on solid residue after HNO_3-HF digestion. [b]HPA digestion on bulk sample. References in the text to isotope values are referred to bulk analyses ([2]) when available or to leached samples in any other case.

case, the trace element, radiogenic isotope, and Mo isotope compositions have been advocated to support the predominant role of recycled sedimentary material into their magma source with no Mo isotope fractionation (Freymuth et al., 2016; Gaschnig et al., 2017). In contrast, in the second two cases the Mo isotope variation from isotopically light to heavy values has been interpreted as due to isotopic fractionation during

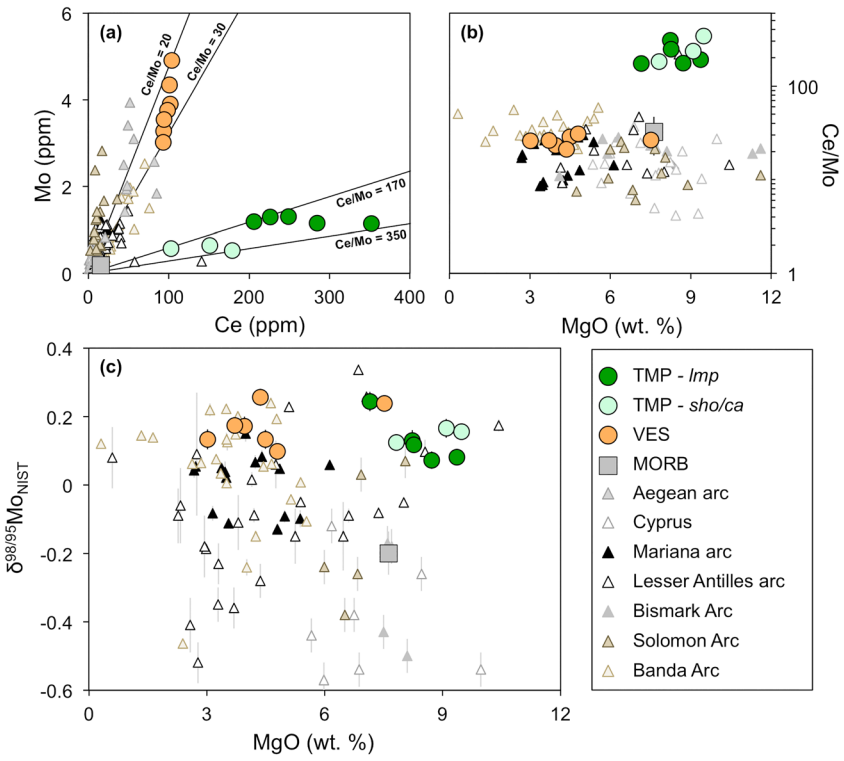

Figure 4. Mo isotope composition and Ce/Mo values of the Tuscan Magmatic Province (TMP) and Mt. Vesuvius magmas along with other subduction-related magmas from literature (Freymuth et al., 2015, 2016; Gaschnig et al., 2017; König et al., 2016; Voegelin et al., 2014; Wille et al., 2018) and MORB average (Gale et al., 2013). (a) Ce versus Mo content (ppm) highlights the opposite behavior of Tuscan Magmatic Province (TMP) and Vesuvius. (b) MgO (wt. %) versus Ce/Mo. (c) MgO (wt. %) versus $\delta^{98/95}$Mo (‰) normalizsed to NIST 3134 of the studied magmas. Error bars (2 s.e., standard error) of the studied samples are smaller than symbol size.

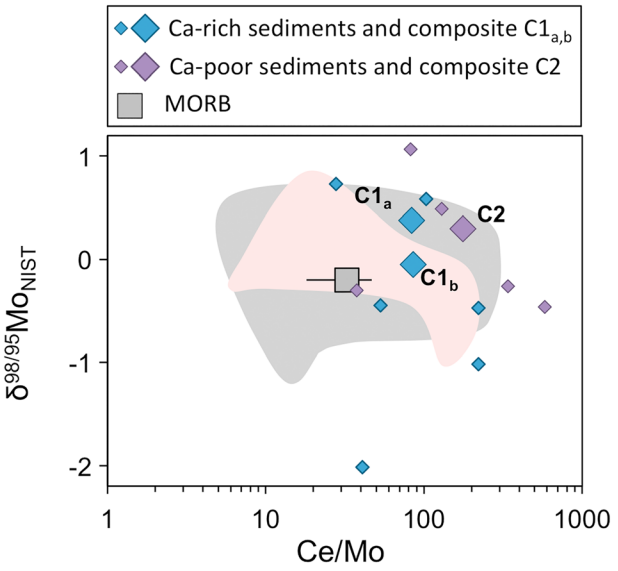

Figure 5. Ce/Mo (log-scale) versus $\delta^{98/95}$Mo (‰) of the Ca-rich and Ca-poor sedimentary materials analyzed, along with the three geochemical composites ($C1_{a,b}$ and C2) calculated in this study. The colored fields represent the sedimentary material of the drilled cores nearby Mariana (light red field) and Lesser Antilles Arcs (gray field; Freymuth et al., 2015, 2016; Gaschnig et al., 2017). Mo isotope composition of MORB is from Freymuth et al. (2015), while its Ce/Mo is the average (±1σ) from Gale et al. (2013).

magmatic differentiation (Voegelin et al., 2014; Wille et al., 2018), although Willbold and Elliott (2017) noted that aspects of the Voegelin et al. (2014) data set were more readily interpreted as magma mixing. These examples illustrate that there is currently no consensus on the processes controlling Mo isotopic compositions at subduction zone settings.

No significant correlation is observed between $\delta^{98/95}$Mo values and MgO content in our data set (Figure 4c). Vesuvius samples show a significant spread in MgO (3.0–7.4 wt. %), which is not coupled with a correlated variation of $\delta^{98/95}$Mo. A trend of increasing $\delta^{98/95}$Mo with decreasing MgO might be inferred for the lamproite Tuscan samples, but these samples are not cogenetic, derived from different locations (Figure 1) and unlikely to be linked by differentiation. Considering the whole data set, the relatively small variation of $\delta^{98/95}$Mo with respect to the large MgO range (9.3–3.0 wt. %) suggests that Mo isotopic compositions of the studied rocks are not controlled by fractional crystallization processes (Figure 4c), although the nature of the sample set makes this assessment undefinitive. This is different from the evidence reported for Kos (Voegelin et al., 2014) and Banda Arc (Wille et al., 2018) but consistent to other volcanic suites (e.g., Casalini, 2018; Freymuth et al., 2015; Gaschnig et al., 2017; König et al., 2016; Yang et al., 2015).

4.2. Sediments

The results of Mo isotopic compositions and Mo concentrations of the sedimentary samples are listed in Table 1 and shown in Figure 5 (with Ce/Mo). The samples are subdivided into siliciclastic (hereafter Ca-poor) and marly (hereafter Ca-rich) lithologies, according to their mineralogy, geochemical composition, and Sr isotope compositions (Figure 3). The two groups are also consistent with previous studies that modeled mantle enrichment processes underneath TMP and Vesuvius (e.g., Figure 3; Avanzinelli et al., 2008, 2009, 2018; Conticelli et al., 2015; Iovine et al., 2018; Peccerillo, 2017).

As a whole, the sedimentary rocks have relatively low Mo contents, with no significant difference between the two lithologies (Ca-rich marls 0.22–0.58 ppm and Ca-poor shale 0.11–1.10 ppm; Table 1) and variable Ce/Mo, which is on average lower for Ca-rich sediments. No systematic trend is observed between Ce/Mo and Mo isotope composition within the Ca-rich group, whereas a slight tendency to higher $\delta^{98/95}$Mo with decreasing Ce/Mo is observable in the Ca-poor group. The overall isotopic composition covers a range of $\delta^{98/95}$Mo values from low 1.01 ± 0.03‰ to high 1.07 ± 0.03‰, greatly exceeding the value of MORB reference ($\delta^{98/95}$Mo value of ~−0.21‰; Bezard et al., 2016), with no systematic differences between the two groups. A single Ca-rich sample displays even lighter values of −2.02 ± 0.04‰. Such isotopic variability, largely independent of lithology, can be tentatively ascribed to the depositional conditions occurring in the ocean, and between the water column and the sea bottom, during sediment deposition. High $\delta^{98/95}$Mo values, inherited from seawater, are recorded in sediments deposited under anoxic to strictly euxinic conditions, while intermediate to low $\delta^{98/95}$Mo values occur in a wide variety of sedimentary materials deposited under oxic-to-slightly anoxic conditions. In our data set, marly rocks represent admixtures between continental-derived clays and seawater carbonates. The former could be driven to isotopically light Mo isotope compositions, according to evidence reported in Archer and Vance (2008) who showed that weathering preferentially removes the heavier Mo isotopes, while the latter should be isotopically heavy according to the values reported in Voegelin et al. (2009). In our data set, however, Ca-poor shales show variable $\delta^{98/95}$Mo, including isotopically heavy values, and in general they are not lighter than Ca-rich marls (Figure 5); this reinforces the notion that local redox conditions of the depositional basin (e.g., basin restriction, productivity upwelling, and occurrence of Fe-Mn nodule fractionation) rather than the lithology exert the main control on Mo isotopes.

Similar isotopic variability within different sediment types had been extensively reported by studies where Mo isotopes are used as oceanic paleoproxy, entailing that the isotopic range defined by sediments deposited under variable suboxic to anoxic conditions covers almost the entire isotopic range comprised

between oxic Fe-Mn nodules and euxinic sediments (see Kendall et al., 2017, for a review). The sediment data from our study are shown in Figure 5 together with those of the sedimentary samples from the Pacific crust (ODP Leg 129; Freymuth et al., 2015, and DSDP Site 144, Freymuth et al., 2016; Gaschnig et al., 2017) to have a comparison with oceanic sediments to be recycled in subduction zones that have been analyzed for Mo isotopes. The sedimentary samples of this study overlap the whole range spanned by literature data (consisting of very low $\delta^{98/95}$Mo pelagic clays, radiolarites, and volcanoclastic sediments, Freymuth et al., 2015, and isotopically heavier calcareous-carbonaceous black shale, Freymuth et al., 2016) slightly extending to higher and lower $\delta^{98/95}$Mo values, although at a slightly less variable Ce/Mo.

Previous studies have estimated the average composition of the subducting component taking into account the thickness and density of each stratigraphic unit (Carpentier et al., 2008; Plank & Langmuir, 1993). In our case this is not possible due to the total consumption of the Tethys ocean lithosphere. Therefore, we attempted to calculate putative sediment composites mixing the different samples from each group using a geochemical criterion. Namely, the two different sediment composites were constructed to attain Sr and Nd isotopic compositions consistent with those of the metasomatizing agents modeled in previous studies for the genesis of the TMP and Vesuvius magmas (dashed fields; Figure 3): (i) a Ca-poor sediment composite for the Tuscan mantle source (e.g., Conticelli, 1998; Conticelli et al., 2009, 2011, 2013) and (ii) a Ca-rich sediment composite for the second step of metasomatism of the Vesuvius mantle source (Avanzinelli et al., 2018). The geochemical and isotopic characteristics of the estimated composites are reported in Tables S1 and S3. Considering the presence in the Ca-rich group of a single sample with extremely low $\delta^{98/95}$Mo, we tentatively calculated two different Ca-rich composites (Figure 5): one excluding the aforementioned anomalous light sample ($C1_a$) and the other including all the samples ($C1_b$).

As a result of the different weighing mixtures to attain the correct Sr and Nd isotopic composition (Figure 3), the two composites have distinct trace element and, obviously, radiogenic isotope compositions (Table S1). In terms of Mo isotopes, however, composite $C1_a$ (Ca rich) and C2 (Ca poor) have similar $\delta^{98/95}$Mo (0.38‰ and 0.30‰, respectively), while $C1_b$ composite yields an obviously lower $\delta^{98/95}$Mo (−0.05‰), due to the effect of the anomalously light sediment sample (Figure 5). In contrast, Ce/Mo is significantly different between the two composites: lower for the two Ca-rich composites (Ce/Mo = 84 and 85 for $C1_a$ and $C1_b$, respectively) and higher for the Ca-poor composite (Ce/Mo = 175). We are aware that these estimates may not represent the actual sedimentary composites recycled in the mantle, but they provide an indication of the overall weighted average composition of such material, which will serve as a starting point, together with the volcanic rock data, to discuss the behavior of Mo (and Ce) in subduction zones.

5. Discussion

It has long been demonstrated (e.g., Avanzinelli et al., 2008, 2009, 2018; Conticelli & Peccerillo, 1992; Gasperini et al., 2002; Iovine et al., 2018; Peccerillo, 1998, 2017, for reviews) that the mantle sources of TMP and Vesuvius magmas are strongly metasomatized by sediment melt components recycled through subduction, which differ in lithology (and thus geochemical and isotopic composition). While Tuscan magmas demand for a mainly siliciclastic (i.e., Ca-poor) sediment, Vesuvius rocks require a two-step process, the second of which must involve marly (i.e., Ca-rich) sediments (Avanzinelli et al., 2018; Figure 3). As highlighted in the previous section (Figure 4), the Ce/Mo and $\delta^{98/95}$Mo are not likely to be affected by crystal fractionation processes. The same holds true for mantle melting, given the similar degree of incompatibility of Mo and Ce (Newsom et al., 1986). For this reason, in the following discussion we will focus on the behavior of these geochemical and isotopic parameters during the subduction-related metasomatic process, considering the above-mentioned different lithologies involved. The striking observation arising from our data is that these magmas have distinct trace element composition, in particular Ce/Mo but broadly similar $\delta^{98/95}$Mo. The same characteristics likely apply to the sediment melt components, which are likely to dominate the trace element and isotopic budget of the mantle source of these highly enriched magmas. This is because these slab-derived metasomatic agents form low melting point components within the metasomatized mantle (i.e., veins; Foley, 1992), which are expected to be totally exhausted and diluted with ambient mantle during mantle melting.

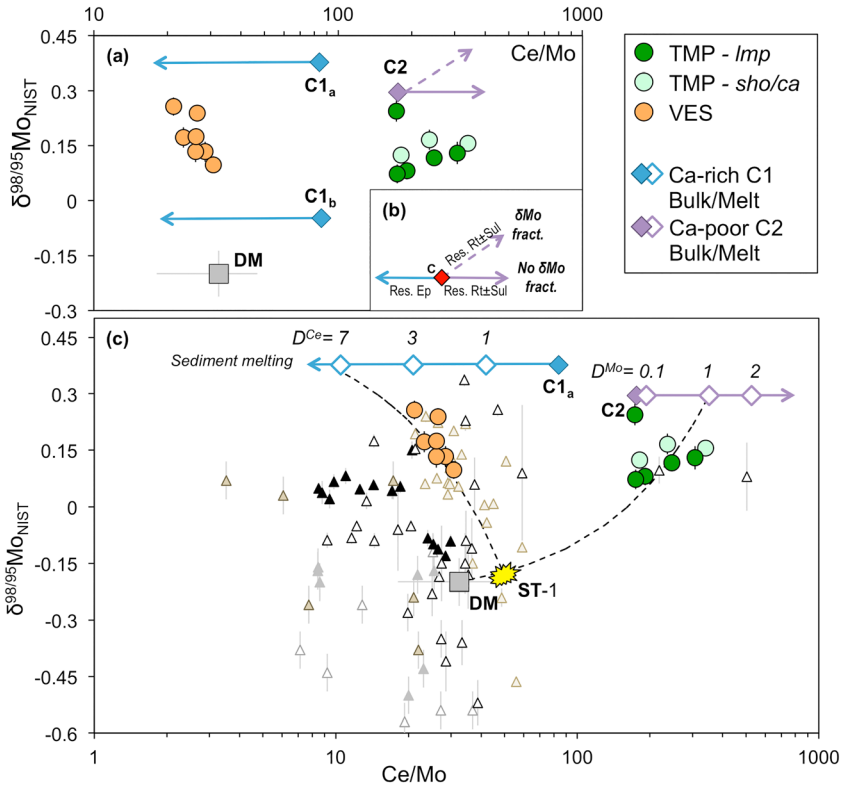

Figure 6. Geochemical model of Ce/Mo (log scale) versus $\delta^{98/95}$Mo (‰) of the sediment-dominated associations of Tuscan Magmatic Province (TMP) and Mt. Vesuvius. Other subduction-related magmas and MORB are reported for comparison (data source as in Figure 4). (a) Expected melting trajectories of the three considered sedimentary composites ($C1_{a,b}$ and C2) as outlined in (b). (b) Schematic outline of partial melting process of a subducted sediment with different residual phases (i.e., Ep: epidote, Rt: rutile, and Sul: sulfide), which are liable to determine Ce/Mo fractionation with (dashed trajectory) or without (solid trajectory) Mo isotope fractionation according to the studies of Freymuth et al. (2015), Skora et al. (2017), and Willbold and Elliott (2017). (c) Ce/Mo (log scale) versus Mo isotope composition for the subduction-related magmas of this study and the bulk (solid diamonds) and melt (open diamonds) compositions of the sedimentary composites representing the metasomatic agents of the Tuscan Magmatic Province (C2) and Vesuvius ($C1_a$) mantle source. Different melt compositions are calculated using different values of D^{Mo} and D^{Ce} (see text for details and Table S3). The overall isotopic compositions of the Tuscan Magmatic Province (TMP) magmas are roughly accounted for by mixing the depleted mantle wedge (DM) and a partial melt (D^{Mo} = 1 and D^{Ce} = 0; F = 50%) of C2 sediment composite. The samples of Vesuvius define a broad linear regression (dashed line, R^2 = 0.57) that can be reproduce by mixing a partial melt of sediment composite $C1_a$ (D^{Mo} = 0 and D^{Ce} = 7; F = 50%) and a mantle end-member previously modified by the addition of siliciclastic sediment melt along the DM-C2 trajectory consistent with the two-step mantle metasomatism recently suggested for Vesuvius magmas (for details see Figure 3 and Avanzinelli et al., 2018). The Depleted Mantle wedge (DM) is assumed to have the same value of Ce/Mo and $\delta^{98/95}$Mo of MORB. Error bars on $\delta^{98/95}$Mo (2 s.e., standard error) of the studied samples are within symbol size.

5.1. Ce/Mo and Sediment Melting

The Ce/Mo calculated for the Ca-poor composite (C2) is higher than that of the Ca-rich composites ($C1_{a,b}$), consistent with the different Ce/Mo of TMP and Vesuvius magmas (Figure 6a). Yet the Ce/Mo of the studied magmas requires further elemental fractionation, in an opposite sense for the two cases. Tuscan rocks require a sediment melt component with Ce/Mo higher than that of the bulk composite C2 (Figure 6a). Vesuvius lavas require, instead, a sediment melt component with Ce/Mo lower than that of the bulk composites C1 (no difference between $C1_a$ and $C1_b$).

Here we attempt to set constraints on the fractionation of Ce from Mo, which is able to reproduce the melt components metasomatizing the mantle wedge and account for the Ce/Mo of TMP and Vesuvius rocks. The fate of Mo isotopes will be discussed in the next section. The difference between the bulk Ce/Mo and the Ce/Mo^{melts} of the sediment components must be related to the different lithologies (C1 vs. C2) and the process of sediment partial melting.

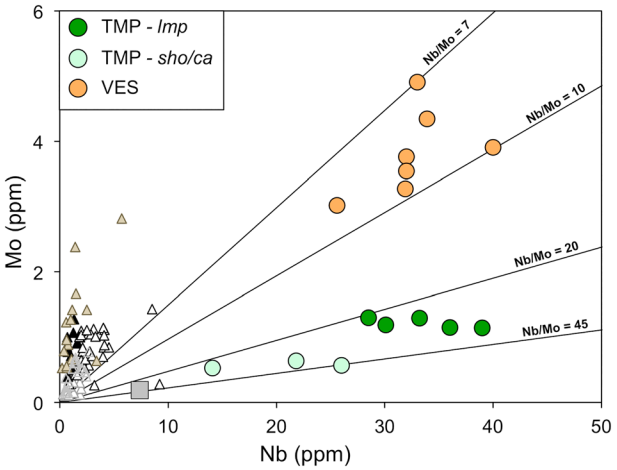

Figure 7. Nb versus Mo content (ppm) of the Tuscan Magmatic Province (TMP) and Mt. Vesuvius magmas along with other subduction-related magmas from literature (Freymuth et al., 2016, 2015; Gaschnig et al., 2017; König et al., 2016; Voegelin et al., 2014; Wille et al., 2018) and MORB average (Gale et al., 2013). Legend as in Figure 4.

Assuming a sediment melting degree of some 50% (e.g., Skora et al., 2015, 2017), we calculated the D^{Mo} and D^{Ce} needed to attain Ce/Mo values in the sediment melt components able to account for the Ce/Mo of the studied samples (Figure 6c). In the case of the Vesuvius magmas, in order to achieve the low inferred Ce/Mo^{melt}, we assume Mo as perfectly incompatible in the residual mineralogy ($D^{Mo} = 0$) and even in this end-ember case Ce needs to be compatible (symbols are shown for $D^{Ce} = 1, 3, 7$ in Figure 6c). Considering a slightly higher D^{Mo} would obviously require a consequent increase in D^{Ce}. This situation requires a residual sediment mineralogy where host phases retain Ce but not Mo, such as epidote group minerals (Skora et al., 2017). Such a behavior is consistent with the findings of two recent studies (i.e., Avanzinelli et al., 2018; Skora et al., 2017), which linked the nature of the residual phases during slab melting to the lithology of the downgoing sediments and the redox conditions. These two parameters are critical in controlling Ce/Mo of sediment melts.

During melting of Ca-rich sediments, high Ca-content and oxidizing conditions allow the stability of epidote group minerals, which strongly retain Ce (along with other REE and Th) but not Mo and produce low Ce/Mo melt components (Ce/Mo = 0.4–13; Skora et al., 2017). In a recent paper, Avanzinelli et al. (2018) demonstrated the key role played by residual epidote during the second step of metasomatism in the mantle source of Vesuvius magmas (including the samples analyzed in this study). These authors, combining U series disequilibria and $\delta^{238/235}U$, suggested that melting of Ca-rich sediments favored the conditions for residual epidote formation, which retained Th over U, and produced a metasomatic agent with elevated ($^{238}U/^{230}Th$) of the order of those observed at Vesuvius. We argue here that the same process can also account for the low Ce/Mo of the metasomatic melt component involved in the mantle source of Vesuvius magmas (Figure 6c).

In the case of TMP magmas, a sediment melt component with Ce/Mo higher than the bulk Ce/Mo of the Ca-poor composite is needed. In this case we assumed $D^{Ce} = 0$ and explored D^{Mo} values required to generate a metasomatic agent able to reproduce the Ce/Mo of the studied magmas. These represent minimum estimates of D^{Mo}. Sediment melt components calculated using different model D^{Mo} ($D^{Mo} = 0.1$, 1, and 2) are shown in Figure 6c. Rutile is considered as the main host phase for Mo in downgoing slab, during both dehydration (Freymuth et al., 2015; König et al., 2016) and sediment melting, with an estimated $D^{Mo}_{Rt} = 4$ (Skora et al., 2017). In our case, however, the observed shift in Ce/Mo requires extremely high D^{Mo} (Figure 6c) that is difficult to ascribe only to the effect of rutile. Indeed, a $D^{Mo} = 1$ implies the presence of 25% residual rutile, which is clearly unrealistic for simple stoichiometric reasons; starting from a sediment with 1 wt.% TiO_2 and assuming 50% partial melting, even if all the TiO_2 was retained in the residue, a maximum of about 2% rutile would be possible. In addition, rutile is also a major repository phase for Nb (and Ta). The absolute Nb content of TMP and Mt. Vesuvius magmas is similar (Figure 7), in contrast to the observed Th content, which controls the $(Th/Nb)_n$ ratio (Figure 2a). A more important role of rutile in the Tuscan magmas would result in lower Nb content than Vesuvius, which is not observed.

This argues against rutile as the key phase responsible for the difference in Ce/Mo between Tuscan and Vesuvius magmas. Accordingly, in the experiments of Skora et al. (2015), residual rutile was observed both for Ca-poor and Ca-rich sediments during melting. Therefore, other residual phases retaining Mo must have been present during sediment melting. In the experiments of Skora et al. (2017), melting of Ca-poor sediments in reducing conditions resulted in the stabilization of also sulfides, which remained stable in the residue. Sulfides represent another preferential host phases for Mo (e.g., Li & Audétat, 2012), and the net partitioning effects in these Ca-poor sediment melts (Skora et al., 2017) can produce Ce/Mo values consistent with those required for the TMP magmas (Figure 6c). It is thus tempting to suggest that sulfides played a major role in producing the high Ce/Mo of the mantle source of Tuscan magmas.

5.2. $\delta^{98/95}$Mo Versus Ce/Mo of TMP and Vesuvius Rocks

The composition of the magmas requires, for both TMP and Vesuvius, a sediment melt component with high $\delta^{98/95}$Mo. This can be attained either assuming a sediment composite with originally high $\delta^{98/95}$Mo or inferring that sediment melting determines isotopic fractionation toward heavier composition.

Although little is known about possible isotopic fractionation during melting, a few studies have suggested that Mo-hosting residual phases might retain light Mo. The proposed residual phases are rutile and/or sulfides (Freymuth et al., 2015; König et al., 2016; Willbold & Elliott, 2017) and cryptic amphibole (Wille et al., 2018). In our case this process can apply only to the Tuscan magmas, where high Ce/Mo is consistent with dominant role of residual sulfides ± rutile, but not to Vesuvius, where low Ce/Mo requires the presence of residual epidote (Figure 6b). For Tuscan rocks, the estimated sediment composite (C2) has already a suitably high $\delta^{98/95}$Mo value. The $\delta^{98/95}$Mo and Ce/Mo composition of TMP magmas can be accounted for by mixing between different melt components of the Ca-poor composite (C2) and the depleted mantle (DM). For the sake of clarity only the mixing line between the sediment melt with $D^{Mo} = 1$ and the depleted mantle has been reported (Figure 6c). The model does not assume any Mo isotope fractionation, which may be favored by the presence of residual sulfides ± rutile. Accounting for this isotopic fractionation, however, would only shift the $\delta^{98/95}$Mo of the sediment melt component to heavier values (Figure 6b), changing only the proportions of such a component added to the mantle wedge.

In the case of Vesuvius, we proposed two possible sediment composites for the second step of mantle metasomatism (Figure 6a): one with high ($C1_a$) and the other with low $\delta^{98/95}$Mo ($C1_b$). As discussed above, the decrease of Ce/Mo requires the dominant role of residual epidote (Figure 6b). Given the incompatibility of Mo in epidote, no significant isotopic fractionation is expected during sediment melting, implying that the low $\delta^{98/95}$Mo of composite $C1_b$ is not suitable to represent the bulk sediment component metasomatizing the mantle source. The Vesuvius samples define a broad linear trend (curved in the semilog diagram of Figure 6c) that intersects the sediment melt component from $C1_a$ composite at Ce/Mo ~ 10 ($D^{Ce} = 7$). The extrapolation of this linear trend to the mantle end-member does not pass through the original depleted mantle (i.e., DM) composition but intersects a point on the DM-C2 mixing line at Ce/Mo ~ 50–60, indicating a mantle end-member previously affected by a limited amount of metasomatism by a Ca-poor sediment melt component. This is consistent with the evidence for a two-step mantle metasomatism arising from U-series disequilibria, long-lived radiogenic isotopes (Sr, Nd, and Pb) and $\delta^{238/235}$U (Avanzinelli et al., 2018). The first step consists of melts from a slab-derived component (basalt + siliciclastic) similar to that metasomatizing the mantle wedge of the neighboring Stromboli volcano. Although no solid constraints can be set on its Ce/Mo and $\delta^{98/95}$Mo, this mainly siliciclastic component can be assumed to be similar to the Ca-poor melt component modeled for the TMP magmas (Figure 6c). The second step consists of melts from a slab-derived marly component ($C1_a$), which is also responsible for ($^{238}U/^{230}Th$)>1 recorded in Mt. Vesuvius magmas (Avanzinelli et al., 2018).

6. Concluding Remarks

The two different volcanic associations of subduction-related potassic and ultrapotassic igneous rocks of TMP and Mt. Vesuvius display among the high $\delta^{98/95}$Mo recorded so far in subduction-related settings and require an isotopically heavy sedimentary component recycled in their mantle source. Despite their similar $\delta^{98/95}$Mo, the two volcanic suites display significantly different Ce/Mo. This requires the occurrence of Ce/Mo fractionation during sediment melting, whose direction depends on both redox conditions and residual mineralogy (sulfides vs. epidote) and the lithology of the subducted sedimentary material undergoing melting (Ca-poor vs. Ca-rich).

Ultrapotassic and potassic leucite-free TMP mafic rocks indicate the presence of a Ca-poor metasomatizing sediment in their mantle source, which must increase its Ce/Mo during partial melting. Residual rutile alone is not sufficient to account for the Ce/Mo value observed in the magmas, and the occurrence of other phases retaining Mo such as sulfide is required.

The Ce/Mo and $\delta^{98/95}$Mo of Vesuvius leucite-bearing volcanic rocks are consistent with a two-step metasomatic process: the first is likely similar to that of TMP, while the second requires the involvement of a Ca-

rich sediment melt component, consistent with the evidence from U-series disequilibria (Avanzinelli et al., 2018). In this case the stabilization of epidote drives the sediment melt to low Ce/Mo values.

In terms of Mo isotopes, the similarity between the two magmatic associations does not provide any evidence for significant Mo isotope fractionation during sediment melting, although this cannot be excluded especially for Ca-poor sediments. Further experiments on the behavior of Mo isotopes during partial melting of natural materials retaining specific residual phases (e.g., rutile, sulfides, or other accessory phases) will be definitively helpful to put stronger constraints on the behaviour of Mo in subduction zones.

Acknowledgments
We deeply thank H. Freymuth and R. Hin for fruitful discussions on various aspects of the paper. Thanks to C. Coath and M. Ulivi for technical support with Mass Spectrometry. Financial support was provided by Progetti di Ricerca di Interesse Nazionale grants 20158A9CBM and 2015EC9PJ5 and by "Pegaso" Doctoral Fellowship at the Universities of Firenze and Pisa. All new data are stored into the EarthChem Library (https://doi.org/10.1594/IEDA/111291). Compiled data (supporting information Tables S1 and S2) are reported in the paper and cited through the text. We thank four anonymous reviewers for constructive comments that helped to improve the manuscript and Janne Blichert-Toft for editorial handling.

References

Ammannati, E., Jacob, D. E., Avanzinelli, R., Foley, S. R., & Conticelli, S. (2016). Low Ni olivine in silica-undersaturated ultrapotassic igneous rocks as evidence for carbonate metasomatism in the mantle. *Earth and Planetary Science Letters*, *444*, 64–74. https://doi.org/10.1016/j.epsl.2016.03.039

Archer, C., & Vance, D. (2008). The isotopic signature of the global riverine molybdenum flux and anoxia in the ancient oceans. *Nature Geoscience*, *1*(9), 597–600. https://doi.org/10.1038/ngeo282

Arnold, G. L., Anbar, A. D., Barling, J., & Lyons, T. W. (2004). Molybdenum isotope evidence for widespread anoxia in mid-Proterozoic oceans. *Science*, *304*(5667), 87–90. https://doi.org/10.1126/science.1091785

Avanzinelli, R., Casalini, M., Elliott, T., & Conticelli, S. (2018). Carbon fluxes form subducted carbonates revealed by uranium excess at Mount Vesuvius, Italy. *Geology*, *46*(3), 259–262. https://doi.org/10.1130/G39766.1

Avanzinelli, R., Elliott, T., Tommasini, S., & Conticelli, S. (2008). Constraints on the genesis of potassium-rich Italian volcanic rocks from U/Th disequilibrium. *Journal of Petrology*, *49*, 195–223.

Avanzinelli, R., Lustrino, M., Mattei, M., Melluso, L., & Conticelli, S. (2009). Potassic and ultrapotassic magmatism in the circum-Tyrrhenian region: Significance of carbonated pelitic vs. pelitic sediment recycling at destructive plate margin. *Lithos*, *113*(1-2), 213–227. https://doi.org/10.1016/j.lithos.2009.03.029

Ayuso, R. A., De Vivo, B., Rolandi, G., Seal, R. R. I. I., & Paone, A. (1998). Geochemical and isotopic (Nd-Pb-Sr-O) variations bearing on the genesis of volcanic rocks from Vesuvius, Italy. *Journal of Volcanology and Geothermal Research*, *82*(1-4), 53–78. https://doi.org/10.1016/S0377-0273(97)00057-7

Bali, E., Keppler, H., & Audetat, A. (2012). The mobility of W and Mo in subduction zone fluids and the Mo–W–Th–U systematics of island arc magmas. *Earth and Planetary Science Letters*, *351*, 195–207. https://doi.org/10.1016/j.epsl.2012.07.032

Barling, J., Arnold, G., & Anbar, A. (2001). Natural mass-dependent variations in the isotopic composition of molybdenum. *Earth and Planetary Science Letters*, *193*(3-4), 447–457. https://doi.org/10.1016/S0012-821X(01)00514-3

Bertine, K. K., & Turekian, K. K. (1973). Molybdenum in marine deposits. *Geochimica et Cosmochimica Acta*, *37*(6), 1415–1434. https://doi.org/10.1016/0016-7037(73)90080-X

Bezard, R., Fischer-Gödde, M., Hamelin, C., Brennecka, G. A., & Kleine, T. (2016). The effects of magmatic processes and crustal recycling on the molybdenum stable isotopic composition of Mid-Ocean Ridge Basalts. *Earth and Planetary Science Letters*, *453*, 171–181. https://doi.org/10.1016/j.epsl.2016.07.056

Carpentier, M., Chauvel, C., & Mattielli, N. (2008). Pb-Nd isotopic contraints on sedimentary input into the Lesser Antilles arc system. *Earth and Planetary Science Letters*, *272*(1-2), 199–211. https://doi.org/10.1016/j.epsl.2008.04.036

Casalini, M. (2018). $^{98}Mo/^{95}Mo$ and $^{238}U/^{235}U$ in lamproites, shoshonites, and high-K calc-alkaline rocks from Western Alps: inferences on their genesis. *Italian Journal of Geosciences*, *137*(3), 465–477. https://doi.org/10.3301/IJG.2018.20

Casalini, M., Avanzinelli, R., Heumann, A., de Vita, S., Sansivero, F., Conticelli, S., & Tommasini, S. (2017). Geochemical and radiogenic isotope probes of Ischia volcano, Southern Italy: Constraints on magma chamber dynamics and residence time. *American Mineralogist*, *102*(2), 262–274. https://doi.org/10.2138/am-2017-5724

Casalini, M., Heumann, A., Marchionni, S., Conticelli, S., Avanzinelli, R., & Tommasini, S. (2018). Inverse modelling to unravel the radiogenic isotope signature of mantle sources from evolved magmas: The case-study of Ischia volcano. *Italian Journal of Geosciences*, *137*(3), 420–432. https://doi.org/10.3301/IJG.2018.05

Cioni, R., Bertagnini, A., Santacroce, R., & Andronico, D. (2008). Explosive activity and eruption scenarios at Somma-Vesuvius (Italy): Towards a new classification scheme. *Journal of Volcanology and Geothermal Research*, *178*(3), 331–346. https://doi.org/10.1016/j.jvolgeores.2008.04.024

Conticelli, S. (1998). The effect of crustal contamination on ultrapotassic magmas with lamproitic affinity: Mineralogical, geochemical and isotope data from the Torre Alfina lavas and xenoliths, Central Italy. *Chemical Geology*, *149*(1-2), 51–81. https://doi.org/10.1016/S0009-2541(98)00038-2

Conticelli, S., Avanzinelli, R., Ammannati, E., & Casalini, M. (2015). The role of carbon from recycled sediments in the origin of ultrapotassic igneous rocks in the Central Mediterranean. *Lithos*, *232*, 174–196. https://doi.org/10.1016/j.lithos.2015.07.002

Conticelli, S., Avanzinelli, R., Marchionni, S., Tommasini, S., & Melluso, L. (2011). Sr-Nd-Pb isotopes from the Radicofani Volcano, Central Italy: Constraints on heterogeneities in a veined mantle responsible for the shift from ultrapotassic shoshonite to basaltic andesite magmas in a post-collisional setting. *Mineralogy and Petrology*, *103*(1-4), 123–148. https://doi.org/10.1007/s00710-011-0161-y

Conticelli, S., Avanzinelli, R., Poli, G., Braschi, E., & Giordano, G. (2013). Shift from lamproite-like to leucititic rocks: Sr–Nd–Pb isotope data from the Monte Cimino volcanic complex vs. the Vico stratovolcano, Central Italy. *Chemical Geology*, *353*, 246–266. https://doi.org/10.1016/j.chemgeo.2012.10.018

Conticelli, S., Guarnieri, L., Farinelli, A., Mattei, M., Avanzinelli, R., Bianchini, G., et al. (2009). Trace elements and Sr–Nd–Pb isotopes of K-rich, shoshonitic, and calc-alkaline magmatism of the Western Mediterranean Region: Genesis of ultrapotassic to calc-alkaline magmatic associations in a post-collisional geodynamic setting. *Lithos*, *107*(1-2), 68–92. https://doi.org/10.1016/j.lithos.2008.07.016

Conticelli, S., Laurenzi, M. A., Giordano, G., Mattei, M., Avanzinelli, R., Melluso, L., et al. (2010). Leucite-bearing (kamafugitic/leucititic) and-free (lamproitic) ultrapotassic rocks and associated shoshonites from Italy: Constraints on petrogenesis and geodynamics. *Journal of the Virtual Explorer*, *36*, 20. https://doi.org/10.3809/jvirtex.2009.00251

Conticelli, S., Melluso, L., Perini, G., Avanzinelli, R., & Boari, E. (2004). Petrologic, geochemical, and isotopic characteristics of potassic and ultrapotassic magmatism in Central-Southern Italy: inferences on its genesis and on the nature of mantle sources. *Periodico di Mineralogia*, *73*(Special issue 1), 135–164.

Conticelli, S., & Peccerillo, A. (1992). Petrology and geochemistry of potassic and ultrapotassic volcanism in central Italy: Petrogenesis and inferences on the evolution of the mantle sources. *Lithos*, *28*(3-6), 221–240. https://doi.org/10.1016/0024-4937(92)90008-M

D'Antonio, M., Civetta, L., & Di Girolamo, P. (1999). Mantle source heterogeneity in the Campanian Region (South Italy) as inferred from geochemical and isotopic features of mafic volcanic rocks with shoshonitic affinity. *Mineralogy and Petrology*, *67*(3-4), 163–192. https://doi.org/10.1007/BF01161520

Elliott, T. (2003). Tracers of the slab. In J. Eiler (Ed.), *Inside the subduction factory*, *Geophysical Monograph Series*, (Vol. 138, pp. 23–45).

Faccenna, C., Becker, T. W., Lucente, F. P., Jolivet, L., & Rossetti, F. (2001). History of subduction and back arc extension in the Central Mediterranean. *Geophysical Journal International*, *145*(3), 809–820. https://doi.org/10.1046/j.0956-540x.2001.01435.x

Foley, S. F. (1992). Vein-plus-wall-rock melting mechanism in the lithosphere and the origin of potassic alkaline magmas. *Lithos*, *28*(3-6), 435–453. https://doi.org/10.1016/0024-4937(92)90018-T

Freymuth, H., Elliott, T., van Soest, M., & Skora, S. (2016). Tracing subducted black shales in the Lesser Antilles arc using molybdenum isotope ratios. *Geology*, *44*(12), 987–990. https://doi.org/10.1130/G38344.1

Freymuth, H., Vils, F., Willbold, M., Taylor, R. N., & Elliott, T. (2015). Molybdenum mobility and isotopic fractionation during subduction at the Mariana arc. *Earth and Planetary Science Letters*, *432*, 176–186. https://doi.org/10.1016/j.epsl.2015.10.006

Gale, A., Dalton, C. A., Langmuir, C. H., Su, Y., & Schilling, J. G. (2013). The mean composition of ocean ridge basalts. *Geochemistry, Geophysics, Geosystems*, *14*, 489–518. https://doi.org/10.1029/2012GC004334

Gaschnig, R. M., Reinhard, C. T., Planavsky, N. J., Wang, X., Asael, D., & Chauvel, C. (2017). The molybdenum isotope system as a tracer of slab input in subduction zones: An example from Martinique, Lesser Antilles Arc. *Geochemistry, Geophysics, Geosystems*, *18*, 4674–4689. https://doi.org/10.1002/2017GC007085

Gasperini, D., Blichert-Toft, J., Bosch, D., Del Moro, A., Macera, P., & Albarede, F. (2002). Upwelling of deep mantle material through a plate window: Evidence from the geochemistry of Italian basaltic volcanics. *Journal of Geophysical Research*, *107*(B12), 2367. https://doi.org/10.1029/2001JB000418

Goldberg, T., Gordon, G., Izon, G., Archer, C., Pearce, C. R., McManus, J., et al. (2013). Resolution of inter-laboratory discrepancies in Mo isotope data: an intercalibration. *Journal of Analytical Atomic Spectrometry*, *28*(5), 724. https://doi.org/10.1039/c3ja30375f

Greber, N. D., Siebert, C., Nägler, T. F., & Pettke, T. (2012). $\delta^{98/95}$Mo values and molybdenum concentration data for NIST SRM 610, 612 and 3134: Towards a common protocol for reporting Mo data. *Geostandards and Geoanalytical Research*, *36*(3), 291–300. https://doi.org/10.1111/j.1751-908X.2012.00160.x

Hawkesworth, C. J., Gallagher, K., Hergt, J. M., & McDermott, F. (1993). Mantle and slab contributions in arc magmas. *Annual Review of Earth and Planetary Sciences*, *21*(1), 175–204. https://doi.org/10.1146/annurev.ea.21.050193.001135

Hawkesworth, C. J., Turner, S. P., Peate, D. W., McDermott, F., & van Calsteren, P. (1997). U–Th isotopes in arc magmas: Implications for element transfer from the subducted crust. *Science*, *276*(5312), 551–555. https://doi.org/10.1126/science.276.5312.551

Iacono-Marziano, G., Gaillard, F., Scaillet, B., Pichavant, M., & Chiodini, G. (2009). Role of non-mantle CO_2 in the dynamics of volcano degassing: the Mount Vesuvius example. *Geology*, *37*(4), 319–322. https://doi.org/10.1130/G25446A.1

Iovine, R. S., Mazzeo, F. C., Wörner, G., Pelullo, C., Cirillo, G., Arienzo, I., et al. (2018). Coupled δ^{18}O-δ^{17}O and ^{87}Sr/^{86}Sr isotope compositions suggest a radiogenic and ^{18}O-enriched magma source for Neapolitan volcanoes (Southern Italy). *Lithos*, *316*, 199–211.

Kendall, B., Dahl, T. W., & Anbar, A. D. (2017). The stable isotope geochemistry of molybdenum. *Reviews in Mineralogy and Geochemistry*, *82*(1), 683–732. https://doi.org/10.2138/rmg.2017.82.16

König, S., Münker, C., Schuth, S., Luguet, A., Hoffmann, J. E., & Kuduon, J. (2010). Boninites as windows into trace element mobility in subduction zones. *Geochimica et Cosmochimica Acta*, *74*(2), 684–704. https://doi.org/10.1016/j.gca.2009.10.011

König, S., Wille, M., Voegelin, A., & Schoenberg, R. (2016). Molybdenum isotope systematics in subduction zones. *Earth and Planetary Science Letters*, *447*, 95–102. https://doi.org/10.1016/j.epsl.2016.04.033

Li, Y., & Audétat, A. (2012). Partitioning of V, Mn, Co, Ni, Cu, Zn, As, Mo, Ag, Sn, Sb, W, Au, Pb, and Bi between sulfide phases and hydrous basanite melt at upper mantle conditions. *Earth and Planetary Science Letters*, *355*, 327–340.

Liang, Y. H., Halliday, A. N., Siebert, C., Fitton, J. G., Burton, K. W., Wang, K. L., & Harvey, J. (2017). Molybdenum isotope fractionation in the mantle. *Geochimica et Cosmochimica Acta*, *199*, 91–111. https://doi.org/10.1016/j.gca.2016.11.023

Newsom, H., White, W., Jochum, K., & Hofmann, A. (1986). Siderophile and chalcophile element abundances in oceanic basalts, Pb isotope evolution and growth of the Earth's core. *Earth and Planetary Science Letters*, *80*(3-4), 299–313. https://doi.org/10.1016/0012-821X(86)90112-3

Noll, P. D. Jr., Newsom, H. E., Leeman, W. P., & Ryan, J. G. (1996). The role of hydrothermal fluids in the production of subduction zone magmas: Evidence from siderophile and chalcophile trace elements and boron. *Geochimica et Cosmochimica Acta*, *60*(4), 587–611. https://doi.org/10.1016/0016-7037(95)00405-X

Neubert, N., Nägler, T. F., & Böttcher, M. E. (2008). Sulfidity controls molybdenum isotope fractionation into euxinic sediments: Evidence from the modern Black Sea. *Geology*, *36*(10), 775–778. https://doi.org/10.1130/G24959A.1

O'Neill, H. S. C., & Eggins, S. M. (2002). The effect of melt composition on trace element partitioning: An experimental investigation of the activity coefficients of FeO, NiO, CoO, MoO_2 and MoO_3 in silicate melts. *Chemical Geology*, *186*(1-2), 151–181. https://doi.org/10.1016/S0009-2541(01)00414-4

Peccerillo, A. (1998). Relationships between ultrapotassic and carbonate-rich volcanic rocks in Central Italy: Petrogenetic and geodynamic implications. *Lithos*, *43*(4), 267–279. https://doi.org/10.1016/S0024-4937(98)00016-4

Peccerillo, A. (2001). Geochemical similarities between the Vesuvius, Phlegraean Fields and Stromboli Volcanoes: Petrogenetic, geodynamic and volcanological implications. *Mineralogy and Petrology*, *73*(1-3), 93–105. https://doi.org/10.1007/s007100170012

Peccerillo, A. (2017). *Cenozoic volcanism in the Tyrrhenian Sea Region* (p. 399). Cham, Switzerland: Springer-Nature. https://doi.org/10.1007/978-3-319-42491-0

Pichavant, M., Scaillet, B., Pommier, A., Iacono-Marziano, G., & Cioni, R. (2014). Nature and evolution of primitive Vesuvius magmas: An experimental study. *Journal of Petrology*, *55*(11), 2281–2310. https://doi.org/10.1093/petrology/egu057

Plank, T. (2005). Constraints from thorium/lanthanum on sediment recycling at subduction zones and the evolution of the continents. *Journal of Petrology*, *46*(5), 921–944. https://doi.org/10.1093/petrology/egi005

Plank, T., & Langmuir, C. H. (1993). Tracing trace elements from sediment input to volcanic output at subduction zones. *Nature*, *362*(6422), 739–743. https://doi.org/10.1038/362739a0

Prelević, D., Cvetkovic, V., & Foley, S. F. (2006). Accretion of arcoceanic lithospheric mantle in Mediterranean: Evidence from lamproites and mantle xenoliths. *European Geosciences Union, General Assembly*, p. 03860.

Prelević, D., & Foley, S. F. (2007). Accretion of arc-oceanic lithospheric mantle in the Mediterranean: Evidence from extremely high-Mg olivines and Cr-rich spinel inclusions in lamproites. *Earth and Planetary Science Letters*, *256*(1-2), 120–135. https://doi.org/10.1016/j.epsl.2007.01.018

Rudnick, R. L., & Gao, S. (2014). Composition of the continental crust. In R. L. Rudnick (Ed.), *Treatise on geochemistry* (Vol. 4, Chapter 4.1, pp. 1–51). Amsterdam, The Netherlands: Elsevier B.V.

Santacroce, R., Bertagnini, A., Civetta, L., Landi, P., & Sbrana, A. (1993). Eruptive dynamics and petrogenetic processes in a very shallow magma reservoir: The 1906 eruption of Vesuvius. *Journal of Petrology*, *34*(2), 383–425. https://doi.org/10.1093/petrology/34.2.383

Savelli, C. (1967). The problem of rock assimilation by Somma-Vesuvius magma. *Contributions to Mineralogy and Petrology*, *16*(4), 328–353. https://doi.org/10.1007/BF00371529

Siebert, C., Nägler, T. F., von Blanckenburg, F., & Kramers, J. D. (2003). Molybdenum isotope records as a potential new proxy for paleoceanography. *Earth and Planetary Science Letters*, *211*(1-2), 159–171. https://doi.org/10.1016/S0012-821X(03)00189-4

Sims, K. W. W., Newsom, H. E., & Gladney, E. S. (1990). Chemical fractionation during formation of Earth's core and continental crust: clues from As, Sb, W and Mo. In H. E. Newsom, & J. H. Jones (Eds.), *Origin of the Earth* (pp. 291–317). Oxford, UK: Oxford University Press.

Skora, S., Blundy, J. D., Brooker, R. A., Green, E. C. R., de Hoog, J. C. M., & Connolly, J. A. D. (2015). Hydrous phase relations and trace element partitioning behaviour in calcareous sediments at subduction-zone conditions. *Journal of Petrology*, *56*(5), 953–980. https://doi.org/10.1093/petrology/egv024

Skora, S., Freymuth, H., Blundy, J., Elliott, T., & Guillong, M. (2017). An experimental study of the behaviour of cerium/molybdenum ratios during subduction: Implications for tracing the slab component in the Lesser Antilles and Mariana Arc. *Geochimica et Cosmochimica Acta*, *212*, 133–155. https://doi.org/10.1016/j.gca.2017.05.025

Vai, F., & Martini, I. P. (Eds) (2013). *Anatomy of an orogen: The Apennines and adjacent Mediterranean basins*. Cham, Switzerland: Springer-Nature.

Voegelin, A. R., Nägler, T. F., Samankassou, E., & Villa, I. M. (2009). Molybdenum isotopic composition of modern and Carboniferous carbonates. *Chemical Geology*, *265*(3-4), 488–498. https://doi.org/10.1016/j.chemgeo.2009.05.015

Voegelin, A. R., Pettke, T., Greber, N. D., von Niederhäusern, B., & Nägler, T. F. (2014). Magma differentiation fractionates Mo isotope ratios: Evidence from the Kos Plateau Tuff (Aegean Arc). *Lithos*, *190*, 440–448.

Vollmer, R. (1976). Rb-Sr and U-Th-Pb systematics of alkaline rocks: The alkaline rocks from Italy. *Geochimica et Cosmochimica Acta*, *40*(3), 283–295. https://doi.org/10.1016/0016-7037(76)90205-2

Washington, H. S. (1906). *The Roman Comagmatic Region*, (p. 57). Washington, D. C: Carnegie Institution of Washington.

Willbold, M., & Elliott, T. (2017). Molybdenum isotope variations in magmatic rocks. *Chemical Geology*, *449*, 253–268. https://doi.org/10.1016/j.chemgeo.2016.12.011

Willbold, M., Hibbert, K., Lai, Y. J., Freymuth, H., Hin, R. C., Coath, C., et al. (2016). High-precision mass-dependent Molybdenum isotope variations in magmatic rocks determined by double-spike MC-ICP-MS. *Geostandards and Geoanalytical Research*, *40*, 389–403.

Wille, M., Nebel, O., Pettke, T., Vroon, P. Z., König, S., & Schoenberg, R. (2018). Molybdenum isotope variations in calc-alkaline lavas from the Banda arc, Indonesia: Assessing the effect of crystal fractionation in creating isotopically heavy continental crust. *Chemical Geology*, *485*, 1–13. https://doi.org/10.1016/j.chemgeo.2018.02.037

Yang, J., Siebert, C., Barling, J., Savage, P., Liang, Y. H., & Halliday, A. N. (2015). Absence of molybdenum isotope fractionation during magmatic differentiation at Hekla volcano, Iceland. *Geochimica et Cosmochimica Acta*, *162*, 126–136. https://doi.org/10.1016/j.gca.2015.04.011

Geochemistry, Geophysics, Geosystems

Supporting Information for

Ce/Mo and Molybdenum Isotope Systematics in Subduction-related Orogenic Potassic Magmas of Central-Southern Italy

M. Casalini[1,2], R. Avanzinelli[1,3*], S. Tommasini[1], T. Elliott[2], and S. Conticelli[1,3,4]

[1] Dipartimento di Scienze della Terra, Università degli Studi di Firenze, Via Giorgio La Pira, 4, I-50121, Firenze, Italy.

[2] School of Earth Sciences, University of Bristol, Wills Memorial Building, Queens Road, Clifton BS8 1RJ, Bristol, United Kingdom.

[3] Istituto di Geoscienze e Georisorse, Consiglio Nazionale delle Ricerche, Via Giorgio, Via Giorgio La Pira, 4, I-50121, Firenze, Italy.

[4] Istituto di Geologia Ambientale e Geoingegneria, Area della Ricerca di Roma 1 - Montelibretti, Via Salaria km 29,300, I-00015 Monterotondo (RM), Italy.

Contents of this file

Additional Supporting Information (Files uploaded separately)

Table S2. Radiogenic isotope compositions (Sr-Nd-Pb) of the studied magmas and sedimentary materials.

Sample name	Eruption date	reference	$^{87}Sr/^{86}Sr$ initial	$^{143}Nd/^{144}Nd$ initial	$^{206}Pb/^{204}Pb$ initial	$^{207}Pb/^{204}Pb$ initial	$^{208}Pb/^{204}Pb$ initial
Tuscan Province							
MVC100	4.10 Ma	*Conticelli et al., 2002*	*0.716723*	*0.512086*	*18.624*	*15.638*	*38.947*
ORC 01	4.10 Ma	*Conticelli et al., 2002*	*0.715791*	*0.512094*	*18.697*	*15.698*	*39.062*
ORC 04	4.10 Ma	*Conticelli et al., 2009*	*0.715691*	*0.512098*	*18.702*	*15.703*	*39.087*
VS 123	1.35 Ma	*Conticelli et al., 2002*	*0.713509*	*0.512183*	*18.707*	*15.701*	*39.096*
VS 114	1.35 Ma	*Conticelli et al., 2002*	*0.715567*	*0.512061*	*18.675*	*15.663*	*38.986*
VS 184	1.30 Ma	*Conticelli et al., 2002*	*0.715882*	*0.512050*	*18.668*	*15.662*	*38.978*
VS 29	0.88 Ma	*Conticelli et al., 2002*	*0.715784*	*0.512117*	*18.675*	*15.678*	*38.915*
VS 28	0.88 Ma	*Conticelli et al., 2002*	*0.715916*	*0.512115*	*18.669*	*15.669*	*38.887*
Vesuvius							
VES 01	1697 A.D.	*Avanzinelli et al., 2018*	*0.707311*	*0.512478*	*19.079*	*15.692*	*39.189*
VES 07	1737 A.D.	*Avanzinelli et al., 2018*	*0.707617*	*0.512465*	*19.009*	*15.688*	*39.131*
VES 18	1858 A.D.	*Avanzinelli et al., 2008*	*0.707437*	*0.512462*	*19.080*	*15.695*	*39.195*
VES 16	1929 A.D.	*Avanzinelli et al., 2018*	*0.707190*	*0.512472*	*19.115*	*15.691*	*39.212*
VES 17	1944 A.D	*Avanzinelli et al., 2008*	*0.707228*	*0.512474*	*19.021*	*15.696*	*39.151*
97VS718b	472-1631 A.D.	*Avanzinelli et al., 2008*	*0.707729*	*0.512458*	*18.912*	*15.685*	*39.050*
95VS135	472-1631 A.D.	*Avanzinelli et al., 2008*	*0.707325*	*0.512477*	*19.078*	*15.696*	*39.191*

Sediments	Lithology		Instrument-Laborator	$^{87}Sr/^{86}Sr$ measured	2 s.e.	$^{143}Nd/^{144}Nd$ measured	2 s.e.	$^{206}Pb/^{204}Pb$	$^{207}Pb/^{204}Pb$	$^{208}Pb/^{204}Pb$
SD 47	*Carbonate-rich marlstone*	*this study*	TIMS - Florence	0.707890	0.000005	0.512099	0.000005			
SD 44	*Carbonate-rich marlstone*	*this study*	TIMS - Florence	0.707973	0.000005	0.512234	0.000005			
SD 48	*Carbonate-rich marlstone*	*Avanzinelli et al., 2018*	TIMS - Florence	*0.708040*		*0.512163*		*18.864*	*15.675*	*38.908*
SD 34	*Carbonate-rich marlstone*	*this study*	TIMS - Florence	0.710656	0.000005	0.512058	0.000005			
SD 53	*Carbonate-rich marlstone*	*this study*	TIMS - Florence	0.709830	0.000006	0.512179	0.000005			
SD 11	*Carbonate-rich marlstone*	*Avanzinelli et al., 2018*	TIMS - Florence	*0.710361*		*0.512205*		*18.851*	*15.679*	*38.910*
SD 41	*Carbonate-poor marlstone*	*this study*	TIMS - Florence	0.719258	0.000005	0.512050	0.000005			
SD 55	*Carbonate-poor marlstone*	*this study*	TIMS - Florence	0.714071	0.000006	0.512113	0.000006			
SD 42	*Carbonate-poor marlstone*	*this study*	TIMS - Florence	0.713876	0.000005	0.512091	0.000005			
SD 75	*Carbonate-poor marlstone*	*this study*	TIMS - Florence	0.721512	0.000006	0.512048	0.000005	*18.612*	*15.597*	*38.755*
SD 62	*Carbonate-poor marlstone*	*this study*	TIMS - Florence	0.729177	0.000005	0.511966	0.000005			

Reproducibility of International Standards	$^{87}Sr/^{86}Sr$ measured	2 σ abs.	#
SRM 987 - within run analyses	0.710248	0.000016	6
SRM 987 - long term reproducibility	0.710248	0.000016	*292*
SRM 987 reference value (Thirlwall, 1991)	*0.710248*	*0.000011*	*427*
AGV1 standard	0.703982	0.000021	*5*
AGV1 reference value (Weis et al., 2006)	*0.703996*	*0.000020*	*10*

Reproducibility of International Standards	$^{143}Nd/^{144}Nd$	2 σ abs.	#
Nd-Fi (internal standard) within run analyses	0.511467	0.000006	3
Nd-Fi long term reproducibility	0.511468	0.000009	165
La Jolla long term reproducibility	0.511846	0.000007	67
La Jolla reference value (Thirlwall, 1991)	*0.511856*	*0.000007*	*44*

Sr and Nd isotopes were measured at the Radiogenic Isotopes Laboratory of the University of Firenze (Avanzinelli et al., 2005) with a Thermo Finnigan Triton Thermal Ionisation Mass Spectrometer (TIMS-UniFi) in multi-dynamic mode (Thirlwall, 1991). Internal errors on sample data (± 2 s.e.) are fully propagated for all the corrections applied. Reproducibility of International Standards is expressed as 2σ; (#) = number of analyses. Numbers in Italic are from already published papers.

Ref:

Avanzinelli, R., Boari, E., Conticelli, S., Francalanci, L., Guarnieri, L., Perini, G., Petrone, C.M., Tommasini, S., & Ulivi, M., (2005), High precision Sr, Nd, and Pb isotopic analyses using the new generation thermal ionisation mass spectrometer thermofinnigan triton-Ti®. Periodico di Mineralogia, 74, 147-166.

Avanzinelli, R., Casalini, M., Elliott, T., & Conticelli, S., (2018), Carbon fluxes form subducted carbonates revealed by uranium excess at Mount Vesuvius, Italy. Geology, 46, 259-262.

Conticelli, S., D'Antonio, M., Pinarelli, L., Civetta, L., (2002), Source contamination and mantle heterogeneity in the genesis of Italian potassic and ultrapotassic volcanic rocks: Sr–Nd–Pb isotope data from Roman Province and Southern Tuscany. Miner. Petrol., 74, 189-222.

Conticelli, S., Guarnieri, L., Farinelli, A., Mattei, M., Avanzinelli, R., Bianchini, G., Boari, E., Tommasini, S., Tiepolo, M., Prelević, D., Venturelli, G. (2009). Trace elements and Sr–Nd–Pb isotopes of K-rich, shoshonitic, and calc-alkaline magmatism of the Western Mediterranean Region: genesis of ultrapotassic to calc-alkaline magmatic associations in a post-collisional geodynamic setting. Lithos, 107(1), 68-92.

Thirlwall, M.F., (1991), Long-term reproducibility of multicollector Sr and Nd isotope ratio analysis. Chemical Geology: Isotope Geoscience section, 94, 85-104.

Weis, D., Kieffer, B., Maerschalk, C., Barling, J., de Jong, J., Williams, G.A., Hanano, D., Pretorius, W., Mattielli, N., Scoates, J.S., Goolaerts, A., Friedman, R.M., Mahoney, J.B., (2006), High-precision isotopic characterization of USGS reference materials by TIMS and MC-ICP-MS. Geochemistry Geophysics Geosystems, 7, Q08006.

Table S3. Sedimentary composite calculation and relative sediment melt composition.

Sample name	Proportion	Mo	$\delta^{98/95}$Mo	Ce	Ce/Mo	Sr	$^{87}Sr/^{86}Sr$	Nd	$^{143}Nd/^{144}Nd$
Carbonate-rich marlstone									
SD 47	*0.0*								
SD 44	*0.3*								
SD 48	*0.1*								
SD 34	*0.1*								
SD 53	*0.1*								
SD 11	*0.4*								
C1a composite		0.40	0.38	33	84	599	0.70851	16	0.51217
C1a sediment melt (F=50%)		0.79	0.38	17	21	399	0.70851	12	0.51217
SD 47	*0.1*								
SD 44	*0.2*								
SD 48	*0.1*								
SD 34	*0.1*								
SD 53	*0.2*								
SD 11	*0.3*								
C1b composite		0.40	-0.05	34	85	592	0.70851	17	0.51217
Carbonate-poor marlstone									
SD 41	*0.5*								
SD 55	*0.1*								
SD 42	*0.1*								
SD 75	*0.3*								
SD 62	*0.1*								
C2 composite		0.37	0.30	64	176	108	0.71944	28	0.51205
C2 sediment melt (F=50%)		0.37	0.30	129	351	181	0.71944	57	0.51205